ADVANCED ELECTRONIC MATERIALS Open Access
www.advelectronicmat.de

Frequency Response of $MAPbI_3$ Perovskites for Photodetection Application

*Sandra Soriano-Díaz, Omar E. Solis, Diego Ramírez-Muñoz, Pablo P. Boix, Juan P. Martínez-Pastor, and Isaac Suárez**

The frequency response of the photocurrent (I_{ph}) generated in perovskite photodetectors is a crucial issue in imaging or telecommunication applications, although it is briefly discussed in the literature. The present work obtains for the first time the complete expression of the I_{ph} generated on $MAPbI_3$ (MA:methylamoniumI) perovskite polycrystalline thin films. A conditioning circuit is used to extract I_{ph} at 1 V of bias voltage under a square-modulated laser excitation with a sensitivity smaller than 1 nW and a linear dynamic range LDR > 200 dB; It allows an accurate determination of the module of I_{ph} together with the phase, which is not usually reported in photodetector systems. The frequency domain analysis reveals that I_{ph} can be modeled by two fractional poles located at low (10 kHz) and high (39–250 kHz) cut-off frequencies. Optimum geometrical parameters and excitation fluence are found for the wider response, resulting for the best device on a cut off frequency up to 250 kHz, and the reproduction of square-modulated optical waves up to 100 kHz. These results represent an important strategy toward the electrical analysis of $MAPbI_3$ (or other perovskite materials) for the design of posterior electronic stages, optimization of devices and determination of their figures of merit.

1. Introduction

$MAPbX_3$ (MA:methylamonium, X = Br, Cl, and I) polycrystalline thin films have attracted significant attention due to their outstanding optoelectronic properties together with the straightforward and low-cost fabrication processes.[1,2] Among other applications, $MAPbX_3$-based devices present extraordinarily high photoconversion efficiencies, which make them a promising and cost-effective alternative to the traditional semiconductors to implement photoconductors, photodiodes, or phototransistors.[3,4] For example, $MAPbI_3$ thin films exhibit ideal properties for photodetection, such as high absorption coefficients above the bandgap and sharp band edges,[5] carrier diffusion lengths longer than 10 μm,[6] and tolerance against crystalline defects.[7] Indeed, an active $MAPbI_3$ layer provides similar responsivity or dynamic range with much thinner films, compared with traditional semiconductors. Moreover, they can be processed from solution, which enables a hybrid integration with other photonic or electronic systems within in a potentially simple and low-cost manner.[8] $MAPbX_3$-based photodetectors are often characterized in terms of their responsivity (R), spectral tunability, high linear dynamic range, fast response time, and low noise.[9–23]

However, the determination of the frequency (f) response of perovskite photodetectors is practically absent in the literature, despite being an important parameter that provides the bandwidth or the upper limit to the speed of the input signal, crucial figures of merit in image processing, data acquisition or telecommunication applications.[12] There are only a few publications where the −3 dB cut-off frequency ($f_{-3\,dB}$) is indicated,[9,12–14] but none of them extracts a useful expression to predict the

S. Soriano-Díaz, D. Ramírez-Muñoz, I. Suárez
Departamento de Ingeniería Electrónica
Escuela Técnica Superior de Ingeniería
Universidad de Valencia
Valencia 46100, Spain
E-mail: isaac.suarez@uv.es

S. Soriano-Díaz, O. E. Solis, P. P. Boix, J. P. Martínez-Pastor, I. Suárez
UMDO+
Instituto de Ciencia de los Materiales
Universidad de Valencia
Valencia 46980, Spain

P. P. Boix
Instituto de Tecnología Química (Universitat Politècnica de València-Agencia Estatal Consejo Superior de Investigaciones Científicas)
Valencia 46022, Spain

The ORCID identification number(s) for the author(s) of this article can be found under https://doi.org/10.1002/aelm.202300833

DOI: 10.1002/aelm.202300833

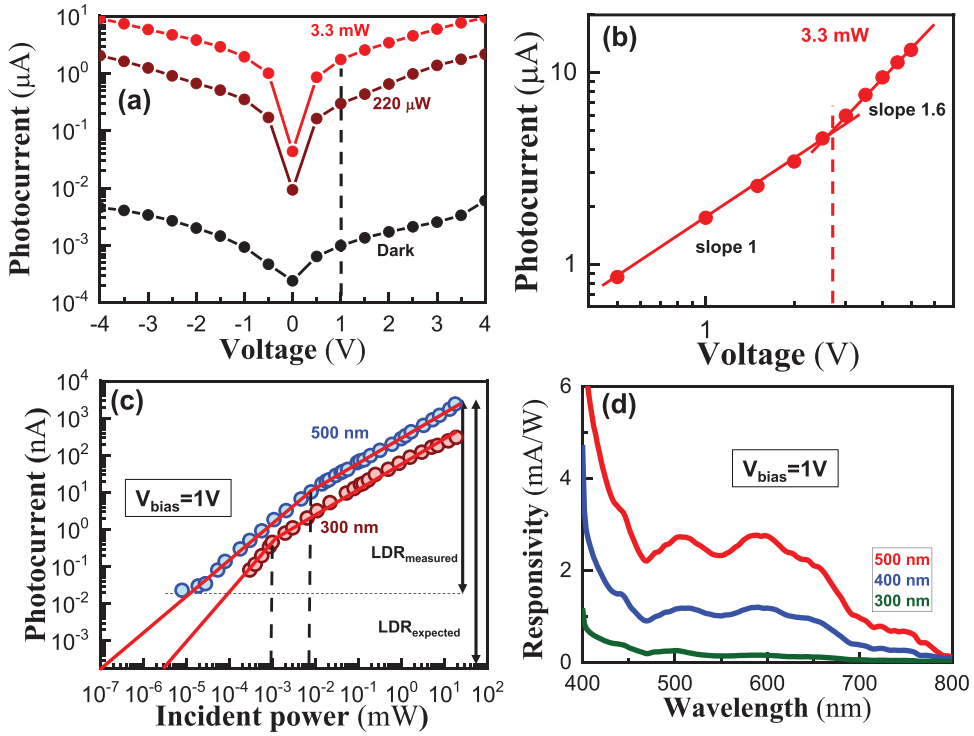

Figure 1. a) I_{ph}–V curve under different light intensities for a sample with d = 500 nm using an excitation laser at 450 nm. b) Log–log plot of the *I–V* curve (V > 0) for P = 3.3 mW. c) Log–log plot of the I_{ph}–P curve for photoconductors with $MAPbI_3$ thicknesses of 500 nm (blue symbols) and 300 nm (brown symbols) using the same laser at 450 nm d) Spectral responsivity for photoconductors with $MAPbI_3$ thicknesses of 500 nm (red), 400 nm (blue) and 300 nm (green).

behavior of the photodevice with f. Nevertheless, its optimization or the design of additional electronic stages composing the full receptor system requires an expression in the complex plane for the generated photocurrent (I_{ph}) versus f, i.e., I_{ph} (jω)/P_{in} (jω), where j is the imaginary number and Ω the angular pulsation ($\omega = 2\ \pi$ f). For this purpose, it is mandatory to obtain experimentally the module of I_{ph} together with the phase-shift ($\Delta\varphi$), which, is not usually reported because its measurement is not directly obtained with conventional electronic systems. Besides, a rigorous estimation of the transfer function requires isolating the influence of the measurement system, which, again, needs the design of an adequate conditioning circuit.

In this work, we determine the photodetection performances of $MAPbI_3$ polycrystalline thin films working in photoconductive mode. The device consists of the perovskite deposited on interdigital electrodes and connected to an appropriate conditioning circuit that supplies the required bias voltage, extracts the generated photocurrent with high sensitivity and filters out the dark current or other undesired noise. At these conditions, the full detector system illuminated with 450 nm light exhibits a high on-off ratio, sensitivity below 1 nW, and photocurrents smaller than 1 nA. Moreover, a frequency modulated spectroscopy technique[24] is successfully applied to obtain the transfer function in the complex plane of I_{ph} generated in the $MAPbI_3$ film, extract the rise/fall times, and the cut-off frequency (80 kHz for the best device). More interestingly, an equivalent circuit model is obtained from this transfer function, which is useful for the future optimization of photodevices or the design of additional electronic stages. This approach is applied to obtain the dependence of the transfer function with the geometrical parameters in several sample configurations and can be extrapolated to other perovskite materials. Thus, these results represent an important step toward understanding the capabilities of $MAPbI_3$ thin films for visible light photodetection and its potential applications in imaging, telecommunications and sensors.

2. Characterization of the Photoconductor

The photodetectors used in this work consisted of a $MAPbI_3$ thin film deposited on a commercial substrate with pre-patterned electrodes, see Figure S1 (Supporting Information) and Experimental Section. The films are formed by compact polycrystalline grains and present good homogeneity, see SEM image in Figure S2 (Supporting Information), and exhibit the ABX_3 crystal structure characteristic of perovskites, see in XRD Figure S3 (Supporting Information). Several sample series were prepared with a fixed electrode gap of g = 50 μm and a $MAPbI_3$ film thickness of d = 300, 400 and 500 nm. As previously reported with $MAPbI_3$ thin films,[5,15] the absorption spectra of the film (see Figure S4, Supporting Information) present a high absorption coefficient greater than 12 μm^{-1} at excitation wavelengths shorter than 550 nm. **Figure 1a** presents the *I–V* curve characterized under dark and continuous wave (CW) illumination of 450 nm for d = 500 nm (the other thicknesses are included in the Figure S5, Supporting Information). The *I–V* curve measured under dark conditions, black symbols in Figure 1a, indicates a dark current,

I_{dark}, smaller than 10 nA and a resistivity between 1800 and 3000 Ω cm, which are similar to values previously published for the same material.[12,15,17,22] The films under CW illumination of 450 nm showed a remarkable photocurrent (I_{ph}), I_{ph}≈1–10 μA, even for low applied bias voltage (<3 V). The carrier mobility calculated with the Mott–Gurney law reaches ≈10^{-2} and ≈1 cm^2 V^{-1} s^{-1} for dark conditions and P = 3.3 mW, respectively, which, again, are in agreement with the values reported for $MAPbI_3$ films elsewhere.[9,16,25] The dark current and photocurrents show a negligible hysteresis when the voltage is sequentially swept from −5 to 5 V and 5 to −5 V, see Figure S5 (Supporting Information). Only the thinner layer (d = 300 nm) exhibits a slight difference in the cyclic *I–V* curves, which can be ascribed to the lower quality due to thickness in the range of the grain size. The log-log plot of the *I–V* curve at P = 3.3 mW, Figure 1b, suggests that the device behaves as a linear ohmic resistance below ≈3 V. This limit corresponds to the required voltage, V_{TFL}, to fill the trap states of the perovskite with the incident carriers and allows us to estimate the density of trap states, n_{trap}, by the equation:[26]

$$n_{\text{trap}} = \frac{2 \times \varepsilon_0 \times \varepsilon_r \times V_{TFL}}{e \times g^2} \quad (1)$$

where ϵ_0 is the vacuum permittivity, ϵ_r the $MAPbI_3$ relative dielectric constant, *g* the channel length and e the elementary charge. Considering $\epsilon_{r=}$ 32 reported for $MAPbI_3$,[27] Equation (1) yields $n_{trap=}$ 4 × 10^{12} cm^{-3}, which is close to the values reported for perovskite thin films measured with microgaps,[28,29] indicating the good crystallinity and homogeneity of the films under study. Thus, to ensure that the device works in the ohmic linear regime, a bias of 1 V is fixed in the following experiments. At the conditions $V_{bias=}$ 1 V, I_{ph} reaches 0.3 and 1.8 μA for P = 220 μW and P = 3.3 mW, respectively. These values correspond to a linear dynamic range (LDR = 20 × log(I_{ph}/I_{dark})) of LDR = 49–65 dB and a responsivity of R = 0.5-1 mA W^{-1}. Nevertheless, the figures of merit of the detector can be further improved with an appropriate electronic circuitry that converts I_{ph} into an accurate signal that can be processed at the downstream stages of the receptor system. With this objective, we propose the use of a transimpedance amplifier, see Figure S6 (Supporting Information), designed to set the operating point to the photoconductor, reduce the noise and discriminate low photocurrent levels on broad bandwidth. The electrical characterization of this circuit indicates an almost constant transimpedance response between direct current (DC) and 775 kHz measured for 1 V of bias voltage under modulated laser excitation at 450 nm, see Figure S7 (Supporting Information), with the required sensitivity to characterize our $MAPbI_3$ photoconductive devices. For this purpose, the electronic components of the circuit were properly optimized to accurately measure the bandwidth of the perovskite photodetector (see next section) and to reduce its dark current. This conditioning circuit was implemented on a printed circuit board (PCB), see Figure S8 (Supporting Information), that converts I_{ph} into a voltage that can be measured either on an oscilloscope or a lock-in amplifier, see Figure S9 (Supporting Information) and experimental Section. The PCB is particularly useful to analyze the photodetection properties under the square modulation of the incident optical beam. In that case, the influence of I_{dark} is prevented, and the overall noise is significantly reduced with a lock-in amplifier. For example, for a modulated signal of 1 kHz and V_{bias} = 1 V, the full detector system (photoconductor + PCB + lock-in) allows an accurate characterization of I_{ph} between P = 8 nW (1.4 μW cm^{-2}) and P = 19 mW (maximum laser fluence, 3.3 W cm^{-2}), see Figure 1c, which resulted on an increased experimental LDR = 73 dB and LDR = 100.7 dB for d = 300 and 500 nm, respectively. Higher LDR can be obtained by extrapolating the measured I_{ph} on the I_{ph}–P curve[12] in Figure 1c, reaching 202 dB for the best device (d = 500 nm), which improves the values reported with many $MAPBI_3$ photodetectors (see Table S1, Supporting Information). More interestingly, the I_{ph}–P curve also indicates an extremely low noise equivalent power, NEP = 0.1 nW (17.5 nW cm^{-2}) for d = 500 nm. At these conditions, the experimental detectivity reaches 3.3 × 10^{11} Jones. Besides, the I_{ph}–P curve presented in Figure 1c evolves from a linear ($I_{ph} \propto P$) to a sublinear ($I_{ph} \propto P^{0.7}$) slope above a threshold power of P = 7.8 μW (1.3 mW cm^{-2}) and P = 1 μW (175 μW cm^{-2}) for d = 500 and 300 nm, respectively, see dashed lines in the figure. This onset corresponds to the transition where the bimolecular recombination becomes dominant over the low carrier injection.[13] Finally, the devices presented the spectral response of the responsivity (R) plotted in Figure 1d, whose shape is similar to that reported for $MAPbI_3$ photodetectors. Again, the photoconductors fabricated with the thicker $MAPbI_3$ films (d = 500 nm) exhibited a better response, with R> 3 mA W^{-1} at 450 nm and an increased R for low excitations (see Figure S10, Supporting Information). Here, the responsivity is reduced to 1–6 mA W^{-1} because of the low bias voltage applied to the electrodes, limited in our study to 1 V to avoid heating or other non-desirable effects.

3. Frequency Response

The electronic interface proposed in the present work is particularly beneficial in the amplification of I_{ph}'s generated by modulated optical beams, commonly applied in imaging, telecommunication or multiplexing applications.[30,31] As discussed in the previous section, the circuit provides an accurate voltage proportional to I_{ph} and with an almost flat response up to 775 kHz. At these conditions, the frequency response of the I_{ph} can be obtained by measuring the circuit voltage with a lock-in amplifier synchronized with the excitation, as depicted in Figure S9 (Supporting Information). In particular, the lock-in amplifier extracts both the amplitude and the phase-shift, Δφ, from the reference of the detected signal, which is required to obtain the transfer function of the system. **Figure 2** presents the frequency response in amplitude (brown symbols) and phase-shift (Δφ, blue symbols) experimentally obtained for three photoconductive devices with d = 500 nm (a,d), 400 nm (b,e) and 300 nm (c,f) illuminated at 3.3 mW (a–c) and 200 μW (d–f). As other photodetector devices,[9,12–14] the amplitude of I_{ph} with f indicates that the devices behave as a low pass filter with a cut-off frequency that depends on the thickness of the $MAPbI_3$ and the excitation fluence. With the optimum conditions of d = 500 nm and P = 3.3 mW the device presents $f_{-3\,dB}$ = 80 kHz, while it decreases down to f_{-3dB}≈10 kHz for the thinner films (d = 300 nm) and smaller excitations (P = 220 μW), see **Table 1**. Since improved crystallization of the $MAPbI_3$ film enhances the bandwidth,[9] we attribute the

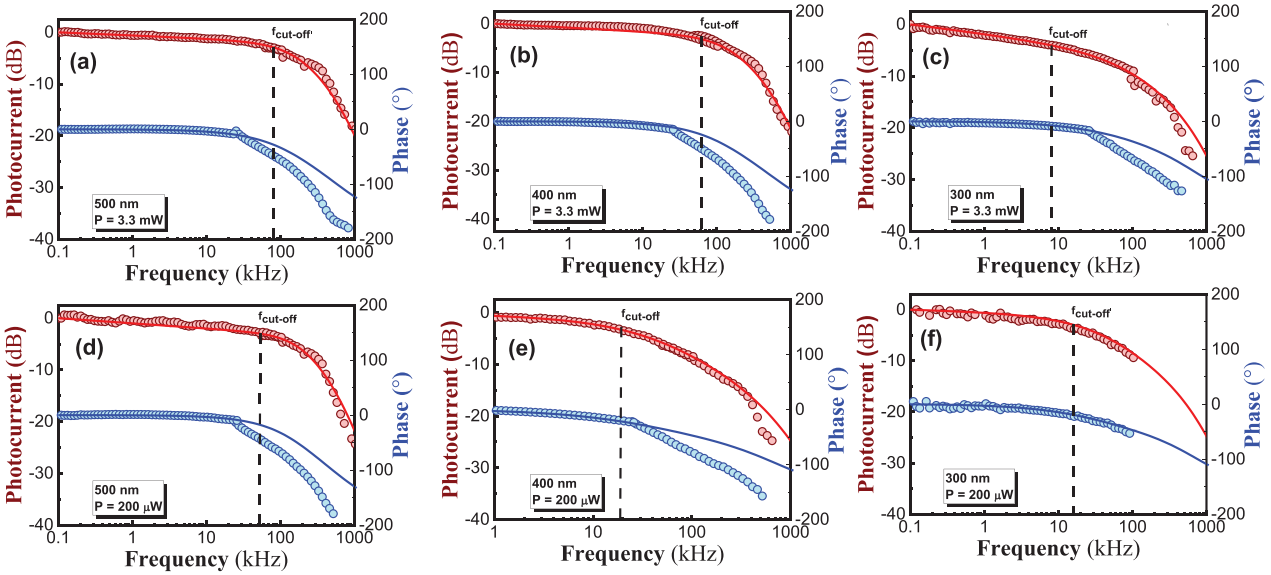

Figure 2. Frequency response of $MAPbI_3$ photoconductor devices under 3.3 mW (a–c) and 200 μW (d–f) and. (a,d) 500 nm, (b,e) 400 nm, (c,f) 300 nm, using a modulated laser at 450 nm. Brown and blue colors correspond to the amplitude and phase-shift of the photocurrent, respectively. Symbols and solid lines refer to the experimental points and the fitting, respectively.

superior −3 dB frequency achieved in thicker films and higher excitation fluence (80 kHz) to the improved layer formation and more intrinsic behaviour of photoconductor. It is worth noting that this value surpasses the typical −3 dB frequency with interdigital electrodes, where the bandwidth is limited to ≈ 10 kHz[19] (refer to Table S1, Supporting Information). This limitation is close to the $f_{-3\,dB}$ measured with our thinner layers (300 nm), 7.6–16.5 kHz. Only more sophisticated configurations, i.e., stacked conductive/electrode layers that reduce the RC-constant between the electrodes and the semiconductor, demonstrate broader cut-off frequencies (> 100 kHz). In the same way, $\Delta\varphi$ follows the low-pass filter response observed with the amplitude: $\Delta\varphi$ is constant for low f, and abruptly decreases above a certain f that depends on the thickness and the excitation fluence.

Moreover, the experimental amplitude/phase I_{ph} of the $MAPbI_3$ thin films used in this work (solid lines in Figure 2b) under different excitation (P = 3.3 mW, 200 μW) and geometrical conditions (d = 500, 400, and 300 nm) can be simulated by a transfer function composed by three fractional poles:

$$\frac{i_{ph}}{i_{ph0}} = \frac{1}{\left(1+\left(j\frac{f}{f_{c1}}\right)^{N1}\right)\times\left(1+\left(j\frac{f}{f_{c2}}\right)^{N2}\right)\times\left(1+\left(j\frac{f}{f_{c3}}\right)^{N3}\right)} \quad (2)$$

Table 1. Spectral response as a function of the thickness and excitation fluence.

d [nm]	$f_{-3\,dB}$ [kHz]	Slope [dB dec^{-1}]	$f_{-3\,dB}$ [kHz]	Slope [dB dec^{-1}]
	P = 3.3 mW		P = 200 μW	
500	80	15.4	52	20.5
400	62	11.2	19.8	6.0
300	7.6	7.5	16.5	5.2

where i_{ph0} is the photocurrent at DC and the fitting parameters f_{ci} and N_i (i = 1,2,3) depend on the thickness of the layer (d) and the excitation fluence (P), see **Table 2**. Since the amplitude and phase depend on the same fitting parameters, a compromise must be found between the amplitude and phase fitting. In this context, we chose to prioritize amplitude over phase, as it plays a crucial role in determining the −3 dB bandwidth of the system. Under these conditions, our modeling accurately reproduces the experimental amplitude, accompanied by a reasonable fitting of the phase until the cut-off frequency, as illustrated by the solid lines in Figure 2. The phase of the proposed model begins to move away from the real for $f > f_{-3\,dB}$. Nevertheless, this deviation from the model is not relevant since the interest of the modeling is in the window $f < f_{-3\,dB}$, where properties of the material are manifested.The parameter i_{ph0} increases with the excitation fluence following the $P^{0.7}$ law deduced in Figure 1c, and the sample volume (i.e., thickness of the film) until saturation above d > 400 nm, see **Figure 3a**. This saturation is attributed to the strong attenuation of the pump at 450 nm along the layer, leading to a negligible excitation above this thickness (i.e., $P(d) \propto e^{-\alpha\cdot d}$, where $\alpha = 12\ \mu m^{-1}$). The three poles $(1+(jf/f_{ci})^{Ni})$ necessary to fit the data indicate three different physical mechanisms

Table 2. Parameters of the transfer function.

P	d [nm]	i_{ph0} [μA]	N_1	f_{c1} [MHz]	N_2	f_{c2} [MHz]	N_3	f_{c3} [MHz]
3.3 mW	500 nm	1	0.06	0.01	0.9	0.25	1	0.775
	400 nm	0.92	0.06	0.01	0.9	0.18	1	0.775
	300 nm	0.08	0.28	0.01	0.9	0.18	1	0.775
200 μW	500 nm	0.17	0.1	0.01	0.99	0.25	1	0.775
	400 nm	0.19	0.018	0.01	0.7	0.039	1	0.775
	300 nm	0.012	0.018	0.01	0.7	0.039	1	0.775

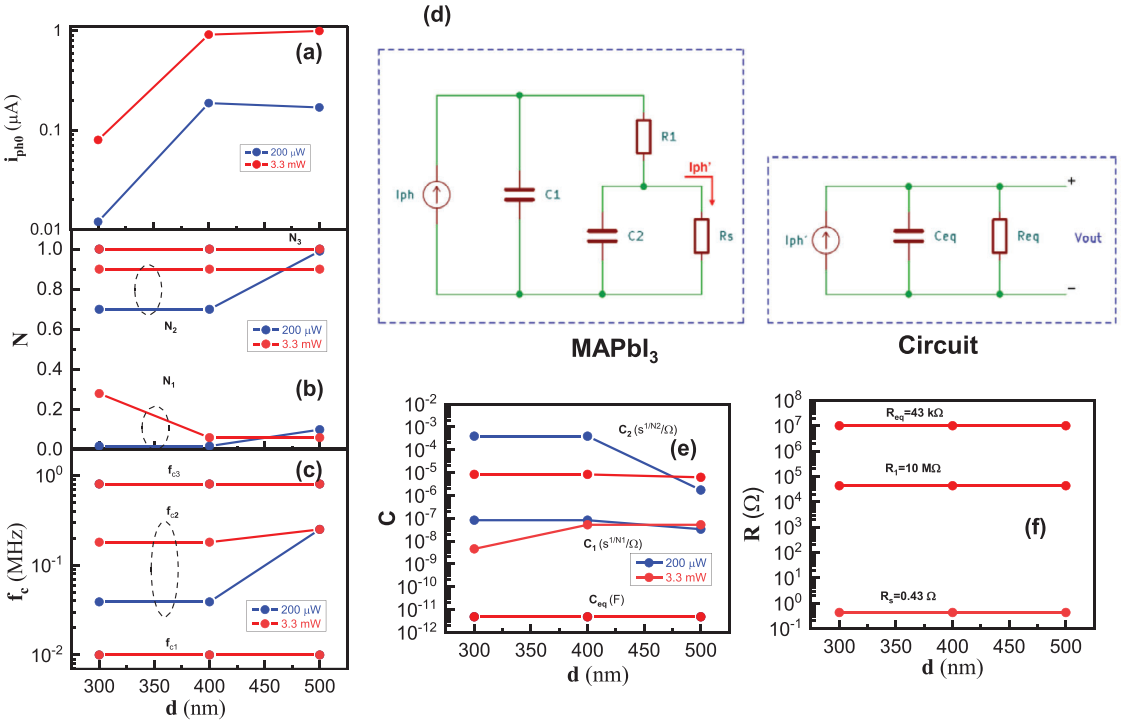

Figure 3. Parameters of the Equation (2) used to fit the data: a) i_{ph0} b) N_1, N_2, N_3 c) f_{c1}, f_{c2}, f_{c3}. d) Equivalent circuit deduced from the transfer function. e) R_1, R_s, R_{eq}. f) C_1, C_2, C_{eq}. Blue and red colors correspond to an excitation of 200 and 3.3 mW, respectively.

influencing the frequency response. Figure 3b,c shows the dependence of N_i and f_{ci} on P and d. There is a low frequency pole fixed at f_{c1} = 10 kHz independently of P and d. The first pole is associated to the non-flat response of I_{ph} below the cut-off frequency, also observed in previous works.[9,12–14] This pole is modeled here with a fixed frequency at f_{c1} = 10 kHz, independently of P and d, and a small exponent (N_1 = 0.1–0.01). The second pole determines the cut-off frequency of the material under study, and it is associated to the intrinsic capacity of the device. The best fitting for this pole is obtained for exponent close to one (N_2 = 0.7–0.99) and a frequency, f_{c2} that increases with P and d from 39 to 250 kHz, see Table II. Finally, the third pole is fixed at f_{c1} = 775 kHz and is ascribed to the RC constant of the conditioning circuit.

The transfer function given by Equation (2) can be synthesized by the equivalent circuit depicted in Figure 3d. For this purpose, it is useful to introduce two stages to separate the contributions of the material under study and the conditioning circuit. The $MAPbI_3$ is modeled by a current source dependent on the excitation fluence (P) and two R-C networks that determine the two pole frequencies. Besides, the conditioning circuit is fixed as the feedback network that sets the transimpedance gain (R_{eq} = 43 kΩ and C_{eq} = 4.3 pF). Figure 3e,f plots each value of R and C obtained from the model as function of the parameters, P, and d. The first RC network is chosen to reproduce the behavior at low frequency (DC-10 kHz). At these conditions, R1 is fixed as the resistance of $MAPbI_3$ measured under CW illumination, which is reported to be 1–10 MΩ,[15] and fixed here to R1 = 10 MΩ according to the *I–V* curve presented in Figure 2. Then, C1 is calculated as the required capacitance to obtain the pole frequency, f_{c1}. For this purpose, the particular shape of the pole requires to introduce a fractional capacitor, i.e., a capacitor with impedance $Z = 1/((j\ \omega)^N\ C)$, commonly used to model the electrical response of not pure electrical systems (vegetables, minerals...).[32] In the $MAPbI_3$ films under study, $C_1 = 10^{-8}$-10^{-7} $s^{N1}\Omega^{-1}$, with N1 = 0.01–0.1, as deduced in Figure 2.[32] Since N1 is close to 0, the first RC network exhibits quasi-resistive behavior, wherein the deviations from a pure resistance reproduce decrease observed in the magnitude of I_{ph} for frequencies below 10 kHz, see Figure 3. Thus, C_1 can be linked to the slow response in photocurrent introduced by shallow traps.[33] On the other hand, the second RC network is introduced to reproduce the behavior of I_{ph} at high frequencies and is correlated with the experimental $f_{-3\ dB}$ obtained in Figure 3.[9,31] Then, this network corresponds to the resistance and capacity of the $MAPbI_3$ film of the circuit in the alternating current regime. By fixing R_S as a shunt resistance R_S = 0.43 Ω, Cs results $Cs = 10^{-6}$-$4\ 10^{-4}$ $s^{N2}\ \Omega^{-1}$, with N2 = 0.7-1, see Figure 2. The exponent N2 close to 1 indicates a quasi-pure capacitive behavior for this fractional capacitor, leading to slope of ≈20 dB per decade above the pole frequency, f_{c2}, that determines the cut-off. Considering N_2≈1 and Cs≈10^{-6} F obtained for d = 500 nm, the time constant derived from this network results on $R_s{\cdot}C_s$ = 0.43 µs, which gives on f≈370 kHz, close to the cut-off frequency deduced from the second network. The deviations from the theoretical value can be ascribed to the transient time (τ_t) of electrons along the photoconductive channel (τ) that decrease the bandwidth by the equation:[31]

$$f_{-3dB}^{-2} = \left(\frac{3.5}{2 \times \pi \times \tau_t}\right)^{-2} + \left(\frac{1}{2 \times \pi \times R \times C}\right)^{-2} \quad (3)$$

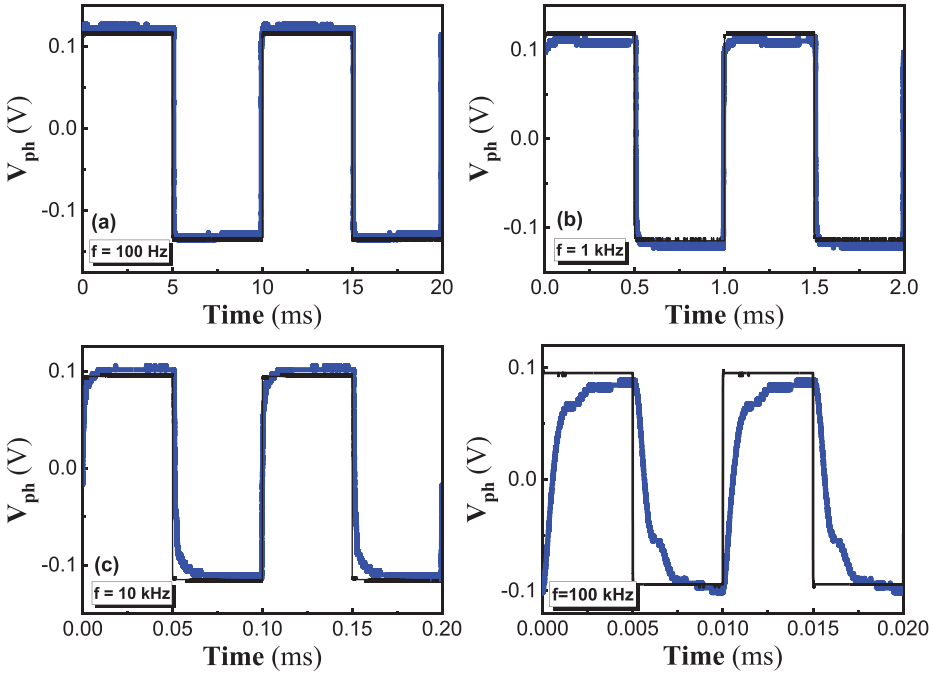

Figure 4. Detector response at a modulated wave of 3 mW (average power). a) 100 Hz, b) 1 kHz, c) 10 kHz and d) 100 kHz.

If $f_{-3\,dB} = 80$ kHz, obtained experimentally for P = 3.3 mW and d = 500 nm, and $1/2\,\pi$ R C = 270 kHz, the transient time reaches $\tau_t = 6.6$ µs. Since our analysis indicates that the RC constant of the $MAPbI_3$ seen by the electrodes is the limiting factor of the frequency response. For this purpose, the strategies proposed in the literature include the improvement of crystallinity of the film[9] or the reduction of the photodetection area.[21,22]

Of course, the narrower bandwidths deduced with the other experimental conditions (P and d) result in longer values for τ_t. More interestingly, the highest electronic mobility (µ), as deduced through the equation $\tau_t = g^2\ (\mu\ V)^{-1}$, is obtained for P = 3.3 mW and d = 500 nm, see Figure S7 (Supporting Information), probably because at these experimental conditions the perovskite presents a better crystallization (thicker layers) and the filling of traps (higher excitation).

The bandwidth obtained from equivalent circuit proposed in Figure 3d predicts the behavior of the device under modulated light used in imaging or telecommunications. Here, the photodetector accurately reproduces square-modulated waves up to 100 kHz, see **Figure 4**, and the wave is only distorted for f > 100 kHz, see Figure S11 (Supporting Information) for f = 1 MHz. Finally, the rise (t_r) and fall (t_f) times derived from the bandwidth can be estimated as $0.35/\ f_{-3\,dB}$, where we believe that f_{c2} determined the behavior of the device rather than the $f_{-3\,dB}$, Indeed, the rise/fall times obtained for f = 100 kHz reaches $t_r = 1.1$ µs and $t_f = 1.5$ µs, see Figure 4, which are giving $f_{-3\,dB} =$ 230–310 kHz, close to f_{c2}.

4. Conclusion

This manuscript analyzes the photodetection response of $MAPbI_3$ perovskites integrated with interdigital electrodes. A conditioning circuit is properly implemented to extract the photocurrents generated under a modulated incident excitation at 450 nm. The electronic components of this circuit were properly optimized for the case of $MAPbI_3$, but it can be redesigned for other materials/devices. At these conditions, we were able to detect signals smaller than 1 nW with 1 V of bias voltage with an expected LDR > 200 dB. More importantly, the analysis of generated photocurrent as a function of the frequency provided a useful expression of the complex transfer function of the material, required for the design of consecutive electronic stages, or to optimize the photodetection properties of the material. This expression reveals that the frequency response of our device is determined by two different mechanisms that can be modeled by fractional poles located at low (10 kHz) and high frequencies (39–250 kHz). The geometrical parameters (i.e., thickness of the layer) and excitation light power impact the bandwidth of the photodetector, up to 250 kHz for the optimum device. These findings contribute to the optimization of $MAPbI_3$ photodetectors for diverse applications where frequency response is a crucial parameter, including, but not limited, to visible communications, medical imaging, and security monitoring.

5. Experimental Section

The $MAPbI_3$ thin films were deposited on a commercial substrate supplied by Ossila. The commercial substrate consisted of a glass pre-patterned with interdigital ITO electrodes supplied by Ossila. The perovskite precursor solution (1.35, 1, and 0.7 M) was prepared by reacting DMF solutions (50 wt%) containing MAI, PbI_2, and DMSO (1:1:1 mol%). Then, 50 µL of this solution was spin-coated inside the glove box, at 4000 rpm (4000 ac) for 50 s. DMF was selectively washed with toluene (as antisolvent) 5–7 s after starting the spin-coating, After the deposition, a ≈500 nm $MAPbI_3$ layer covered the interdigital electrodes, see the grey area in Figure S1 (Supporting Information). The perovskite

film showed the deep brown, highly dense, shiny, and homogeneous morphology characteristic of the $MAPbI_3$ perovskite and exhibited good stability during the measurements.

The photocurrent was measured under ambient conditions at room temperature placing the sample on an Ossila test board (P2008A1) connected to the appropriate system. The *I–V* curves were characterized by illuminating the samples with a continuous wave (CW) 450 nm laser with intensity ranging between 40 and 3 mW with neutral density filters and recording the photogenerated current as a function of the bias voltage using a Keithley Series 2400 Source Meter Unit (Keithley Instruments Inc). The area of the spot was 9.4×10^{-3} cm^2.

To characterize the frequency response, the samples were illuminated with a laser at 450 nm (MDL-XS-450, CNI laser) and its amplitude was externally modulated from 100 Hz to 2 MHz by a signal generator (TTI, model TPG3151). Here, a printed circuit board (PCB) was implemented to discriminate small signals and to analyze their evolution with the modulating frequency. The PCB was designed to provide the required bias voltage to the electrodes to convert the photocurrent I_{ph} generated by the MHP in an alternating voltage that can be measured by an external SR810 DSP lock-in amplifier (Stanford Research Systems) or a digital scope MSO500 (Rigol). The area of the spot was 5.6×10^{-3} cm^2.

Supporting Information

Supporting Information is available from the Wiley Online Library or from the author.

Acknowledgements

This project received funding from the Spanish MINECO through projects no. PID2020-120484RB-I00 and PID2019-107314RB-I00 (Stable). This study also forms part of the Advanced Materials (project no. MFA/2022/066) and Quantum Communication (projects no. COMCUANTICA/009) programmes and was supported by MCIN with funding from European Union Next Generation EU (PRTR-C17.I1) and by Generalitat Valenciana.

Conflict of Interest

The authors declare no conflict of interest.

Data Availability Statement

The data that support the findings of this study are available from the corresponding author upon reasonable request.

Keywords

frequency response, $MAPbI_3$, photodetector, transimpedance amplifier

Received: November 28, 2023
Revised: February 5, 2024
Published online: March 27, 2024

[1] Q. Chen, N. De Marco, Y. Yang, T.-B. Song, C.-C. Chen, H. Zhao, Z. Hong, H. Zhou, Y. Yang, *Nano Today* **2015**, *10*, 355.
[2] H. Zhu, Y. Fu, S. Jin, M. P. Hautzinger, J. Chen, X. Y. Zhu, *Nat. Rev. Mater.* **2019**, *4*, 169.
[3] F. P. García De Arquer, A. Armin, P. Meredith, E. H. Sargent, *Nat. Rev. Mater.* **2017**, *2*, 16100.
[4] G. Li, Y. Wang, L. Huang, W. Sun, *ACS Appl. Electron. Mater.* **2022**, *4*, 1485.
[5] S. De Wolf, J. Holovsky, S. J. Moon, P. Löper, B. Niesen, M. Ledinsky, F. J. Haug, J. H. Yum, C. Ballif, *J. Phys. Chem. Lett.* **2014**, *5*, 1035.
[6] D. Shi, V. Adinolfi, R. Comin, M. Yuan, E. Alarousu, A. Buin, Y. Chen, S. Hoogland, A. Rothenberger, K. Katsiev, Y. Losovyj, X. Zhang, P. A. Dowben, O. F. Mohammed, E. H. Sargent, O. M. Bakr, *Science* **2015**, *347*, 519.
[7] D. Meggiolaro, S. G. Motti, E. Mosconi, A. J. Barker, J. Ball, C. Andrea Riccardo Perini, F. Deschler, A. Petrozza, F. De Angelis, *Energy Environ. Sci.* **2018**, *11*, 702.
[8] Z. Xu, X. Han, W. Wu, F. Li, R. Wang, H. Lu, Q. Lu, B. Ge, N. Cheng, X. Li, G. Yao, H. Hong, K. Liu, C. Pan, *Light Sci. Appl.* **2023**, *12*, 67.
[9] Z. Li, L. Jiang, X. Rong, Q. Dong, H. Dong, L. Wang, G. Dong, *J. Phys. Chem. Lett.* **2022**, *13*, 815.
[10] Z. Lan, L. Cai, D. Luo, F. Zhu, *ACS Appl. Mater. Interfaces* **2021**, *13*, 981.
[11] G. Wu, R. Fu, J. Chen, W. Yang, J. Ren, X. Guo, Z. Ni, X. Pi, C. Z. Li, H. Li, H. Chen, *Small* **2018**, *14*, 1802349.
[12] Q. Lin, A. Armin, D. M. Lyons, P. L. Burn, P. Meredith, *Adv. Mater.* **2015**, *27*, 2060.
[13] Q. Lin, Q. Lin, A. Armin, P. L. Burn, P. Meredith, *Nat. Photonics* **2015**, *9*, 687.
[14] Y. Fang, Q. Dong, Y. Shao, Y. Yuan, J. Huang, *Nat. Photonics* **2015**, *9*, 679.
[15] I. Suárez, E. Hassanabadi, A. Maulu, N. Carlino, C. A. Maestri, M. Latifi, P. Bettotti, I. Mora-Seró, J. P. Martínez-Pastor, *Adv. Opt. Mater.* **2018**, *6*, 1800201.
[16] J. Wang, S. Xiao, W. Qian, K. Zhang, J. Yu, X. Xu, G. Wang, S. Zheng, S. Yang, *Adv. Mater.* **2021**, *33*, 2005557.
[17] M. I. Saidaminov, M. A. Haque, M. Savoie, A. L. Abdelhady, N. Cho, I. Dursun, U. Buttner, E. Alarousu, T. Wu, O. M. Bakr, *Adv. Mater.* **2016**, *28*, 8144.
[18] L. Li, Y. Deng, C. Bao, Y. Fang, H. Wei, S. Tang, F. Zhang, J. Huang, *Adv. Opt. Mater.* **2017**, *5*, 1700672.
[19] G. Li, R. Gao, Y. Han, A. Zhai, Y. Liu, Y. Tian, B. Tian, Y. Hao, S. Liu, Y. Wu, Y. Cui, *Photonics Res* **2020**, *8*, 1862.
[20] C. Li, J. Lu, Y. Zhao, L. Sun, G. Wang, Y. Ma, S. Zhang, J. Zhou, L. Shen, W. Huang, *Small* **2019**, *15*, 1903599.
[21] L. Dou, Y. M. Yang, J. You, Z. Hong, W. H. Chang, G. Li, Y. Yang, *Nat. Commun.* **2014**, *5*, 5404.
[22] Y. Fang, J. Huang, *Adv. Mater.* **2015**, *27*, 2804.
[23] R. Dong, Y. Fang, J. Chae, J. Dai, Z. Xiao, Q. Dong, Y. Yuan, A. Centrone, X. C. Zeng, J. Huang, *Adv. Mater.* **2015**, *27*, 1912.
[24] J. Navarro-Arenas, I. Suárez, A. F. Gualdrón-Reyes, I. Mora-Seró, J. Bisquert, J. Martínez-pastor, *Adv. Opt. Mater.* **2021**, *9*, 2100807.
[25] M. Ahmadi, T. Wu, B. Hu, *Adv. Mater.* **2017**, *29*, 1605242.
[26] Z. X. Zhang, C. Li, Y. Lu, X. W. Tong, F. X. Liang, X. Y. Zhao, D. Wu, C. Xie, L. B. Luo, *J. Phys. Chem. Lett.* **2019**, *10*, 5343.
[27] E. Berger, J. Wiktor, A. Pasquarello, *J. Phys. Chem. Lett.* **2020**, *11*, 6279.
[28] A. D. Densities, H. Perovskite, T. Films, S. Crystals, *ACS Energy Lett.* **2021**, *6*, 3244.
[29] W. Zheng, R. Lin, Z. Zhang, Q. Liao, J. Liu, F. Huang, *Nanoscale* **2017**, *9*, 12718.
[30] C. Li, H. Wang, F. Wang, T. Li, M. Xu, H. Wang, Z. Wang, X. Zhan, W. Hu, L. Shen, *Light Sci. Appl.* **2020**, *9*, 31.
[31] J. Liu, J. Jiang, S. Wang, T. Li, X. Jing, Y. Liu, Y. Wang, H. Wen, M. Yao, X. Zhan, L. Shen, *Small* **2021**, *17*, 2101316.
[32] S. I. R. Arias, D. R. Muñoz, J. S. Moreno, S. Cardoso, R. Ferreira, P. J. P. Freitas, *Sensors* **2013**, *13*, 17516.
[33] A. Maulu, J. Navarro-Arenas, P. Rodríguez-Cantó, J. Sánchez-Royo, R. Abargues, I. Suárez, J. Martínez-Pastor, *Nanomaterials* **2018**, *8*, 677.